

Research on Removing Image Noise and Distortion in Machine Dial Recognition

Xiaoyuan Wang, Hefei University, China

Hongfei Wang, Sinosoft Company Limited, China

Jianping Wang, Hefei University of Technology, China

Maoyu Zhao, Hefei University, China

Hui Chen, Hefei University, China

ABSTRACT

This study aims to address the issues of image noise and distortion in machine dial recognition via initial denoising. A wavelet local threshold denoising method that combines high-frequency wavelet coefficients with wavelet decomposition coefficients in various directions is proposed. This method shows good results on 102 images of car dashboards, aircraft instrument panels, spacecraft displays, and dial instruments on robots. Although a few denoised images exhibit distortion due to intense lighting or heavy contamination, the denoising accuracy for the remaining images is 98.04%, demonstrating substantial practical value. Future research will concentrate on addressing complex image noise and structures.

KEYWORDS

Application, Remove Image Noise and Distortion, Wavelet Transform

Image denoising is a crucial image processing technique to eliminate noise from images, enhance their quality, and render them more suitable for subsequent processing and analysis. Its goal is to reduce or eliminate noise in images through appropriate algorithms and techniques, while preserving or restoring image details and structure. Image denoising techniques find widespread applications in fields such as computer vision, medical imaging, and remote sensing. Traditional image denoising methods include filter-based and wavelet-based approaches (Duan & An, 2021). Filter-based methods, such as mean filtering, median filtering, and Gaussian filtering, are simple and fast, but they aren't very effective against complex noise (Yuan et al., 2022). Wavelet-based methods perform well in addressing high-frequency noise in images.

Currently, many classic and innovative image denoising approaches exist (Wan & Hao, 2022). For example, regarding wavelet transform for image denoising, Zhao, X. (2023) investigated adaptive image denoising by leveraging wavelet transform and sparse representation techniques, enhancing the noise removal efficiency. Abudurehman, A. (2023) also carried out a comparative analysis of various wavelet thresholding techniques, evaluating their image denoising effectiveness and providing insights

DOI: 10.4018/IJITSA.343047

*Corresponding Author

This article published as an Open Access article distributed under the terms of the Creative Commons Attribution License (<http://creativecommons.org/licenses/by/4.0/>) which permits unrestricted use, distribution, and production in any medium, provided the author of the original work and original publication source are properly credited.

into optimal choices for different scenarios. These two studies focus on the application of wavelet transform methods, achieving adaptive image denoising and conducting a comparative analysis of different wavelet thresholding techniques for effective noise removal.

In this paper, we introduce a novel image denoising method that improves upon traditional techniques and addresses the challenges of image denoising in real-world scenarios. It provides innovative methods and technical support to enhance the denoised image quality. The aforementioned research has provided outstanding contributions in the field of image denoising, demonstrating significant achievements. However, further research is needed, particularly to handle complex noise, preserve image details, and refine structural denoising (Yan et al., 2022).

In this paper, we propose a novel image denoising method by integrating features from high-frequency wavelet coefficients with wavelet decomposition coefficients in different directions. We derive a wavelet local threshold denoising approach by comparing the thresholds for multiple wavelet coefficients. The advantage of this image denoising method over conventional wavelet denoising lies in its ability to handle high-frequency information in different directions more accurately, enhancing denoising effectiveness while preserving essential image details and structural features. In practical applications, the wavelet local threshold denoising method can significantly enhance the denoising effectiveness of car, airplane, and robot dashboard images, thereby improving the quality and readability of these images. This enhancement increases the accuracy and reliability of visualization and detection tasks within their respective domains, playing a crucial role in accurate image recognition in subsequent stages (Sun & Feng, 2022).

The proposed wavelet local threshold denoising method holds vast application potential and substantial practical significance in various fields. First, in the realm of image processing, this method can effectively enhance image quality by precisely handling high-frequency information in different directions. It can play a crucial role in improving clarity in medical imaging, satellite imagery, and similar domains (Lv et al., 2021). Second, in signal processing and communication, the application of this method can enhance signal transmission quality, mitigate noise interference in communication systems, and contribute to the overall information transfer reliability. Overall, this method demonstrates outstanding performance in handling complex data, thus providing practical significance and value in data processing and analysis across diverse domains (Yan et al., 2021).

MATERIALS AND METHODS

Wavelet-Based Multiresolution Analysis

Wavelet analysis is a branch of mathematics that combines functional analysis, spline analysis, harmonic analysis, Fourier analysis, and numerical analysis. It has provided significant breakthroughs in nonlinear fields, such as signal processing, image processing, speech analysis, pattern recognition, and quantum physics (Sun & Cui, 2020). In 1988, Stéphane Georges Mallat and Yves Meyer introduced the concept of multiresolution analysis for the construction of orthogonal wavelet bases, clearly illustrating the wavelet's multiresolution characteristics from a spatial perspective (Yan et al., 2020). Mallat and Myer combined all previous methods for constructing orthogonal wavelet bases to propose a method for constructing orthogonal wavelets and a fast orthogonal wavelet transform method, which is known as the Mallat fast wavelet algorithm. This algorithm holds a seminal position in wavelet analysis that is similar to that of the fast Fourier transform algorithm in classical Fourier analysis (Sun et al., 2020).

Denoising plays a crucial role in the field of image processing and computer vision. First, denoising helps to enhance image quality and visual perception, making images clearer and easier to understand. Second, it contributes to improving the accuracy and robustness of subsequent image processing tasks, such as object detection and image segmentation.

However, existing denoising techniques still have some shortcomings. Some methods may remove noise at the expense of losing image details, resulting in blurred or distorted images. Other methods may not perform well on certain types of noise, such as texture or speckle. Additionally, some methods may require a significant amount of computational resources or complex parameter tuning, making them less efficient or easy to implement. Therefore, discussing the existing denoising techniques and their shortcomings is crucial for identifying the development direction of new methods and improving existing ones. By analyzing the pros and cons of existing techniques, we can place the contribution of new methods within the broader research framework, providing guidance and insights for further advancements in the field of image processing (Yan, 2023).

The structure diagram of a three-layer multiresolution tree is shown in Figure 1. The purpose of this tree is to provide guidance for constructing orthogonal wavelet bases that closely approximate the $L^2(\mathbb{R})$ space in terms of frequency, while filters with different bandwidths are equivalent to orthogonal wavelet bases with varying frequency resolutions. The figure shows that the multiresolution analysis does not consider the high-frequency part, but only deeply decomposes the low-frequency part. The relationship is $H = C3 + B3 + B2 + B1$.

Defining Multiresolution

Multiresolution analysis in space $L^2(w)$ refers to a sequence of spaces: $\{G_k\}_{k \in \mathbb{Z}}$ in $L^2(W)$ ($L^2(W)$ is a square-integrable real space, as well as a signal space with finite energy, that satisfies the following conditions: approximability, scalability, monotonicity, translation invariance, and existence of Riesz bases.

Approximability is calculated using the formula shown in equation (1):

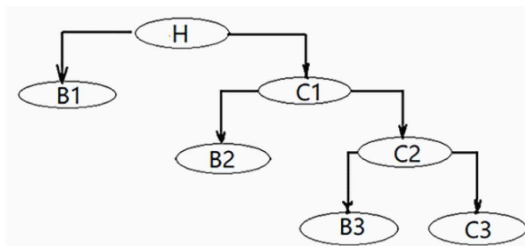
$$\bigcap_{k \in \mathbb{Z}} G_k = \{0\}, \text{close} \left\{ \bigcup_{k=-\infty}^{\infty} G_k \right\} = L^2(W) \tag{1}$$

Scalability is calculated using the formula shown in equation (2):

$$f(t) \in G_k \Leftrightarrow f(2t) \in G_{k+1} \tag{2}$$

This condition reflects the consistency of scale changes, nearly orthogonal wavelet transformations, and spatial variations.

Monotonicity is calculated using the formulas shown in equations (3) and (4):



Note. Source: Hu, et al. (1999), p. 18.

$$G_k \subset G_{k+1} \tag{3}$$

for any:

$$k \in X \tag{4}$$

Translation invariance is calculated using the formula shown in equation (5).

For any $l \in X$, there are:

$$\delta_k(2^{-k/2}t) \in G_k \Rightarrow \delta_k(2^{-k/2}t - 1) \in G_k \tag{5}$$

Existence of Riesz bases is calculated using the formulas shown in equations (6) and (7):

$$\text{Exist } \delta(t) \in G_0 \tag{6}$$

$$\text{Lead to } \left\{ \delta(2^{-k/2}t - 1) \mid 1 \in X \right\} \tag{7}$$

Equations (6) and (7) yield the Riesz basis that constitutes G_k .

Suppose that the low-frequency and high-frequency parts B_k and C_k in the analysis tree decomposition are represented by G_k and P_k , respectively. Subsequently, P_k is the orthogonal complement of G_k in G_{k+1} , as shown in equation (8):

$$G_k \oplus P_k = G_{k+1}, k \in X \tag{8}$$

Therefore, the formula in equation (9) can now be used:

$$G_k \oplus P_k \oplus P_{k+1} \oplus \dots \oplus P_{k+m} = G_{k+m} \tag{9}$$

From equation (9), it can be deduced that the subspace G_0 of the multiresolution analysis can be approximated by a finite subspace, as shown in equation (10):

$$G_0 = G_1 \oplus P_1 = G_2 \oplus P_2 \oplus P_1 = G_N \oplus P_N \oplus P_{N-1} \oplus \dots \oplus P_2 \oplus P_1 \tag{10}$$

Thus, space sequence $\{P_k \mid k \in X\}$ has the nature shown in equations (11)–(13):

$$f(t) \in P_k \Rightarrow f(t - 2^k n) \in P_k, n \in X \tag{11}$$

$$f(t) \in P_k \Leftrightarrow f(2t) \in P_{k+1}, k \in X \tag{12}$$

$$H_{p,f} \Rightarrow 0, \text{ when } |k| \Rightarrow \infty \quad (13)$$

Similar to G_k , a function for the set $\mathcal{f}(t) \in P_0$ is sought by randomly selecting from $f \in L^2(W)$. For each $k \in X$, a space P_k is formed with a standard orthogonal basis function set $\{\mathcal{f}_{k,n} \mid n \in X\}$, as calculated in the formula shown in equation (14):

$$\mathcal{f}_{k,n}(t) = 2^{-k/2} \mathcal{f}(2^{-k}t - n) \quad (14)$$

Now, let $f_k \in G_k$ represent the approximation of $f \in L^2(W)$ at a resolution 2^{-k} obtained using G_k . It also represents the low-frequency component of the function f and corresponds to a “coarse image.”

When $C_k \in P_k$ is used, the error of the approximation also represents the high-frequency component of the function f , which corresponds to the image “details.”

Therefore, equation (10) can be interpreted as shown in equation (15):

$$f_0 = f_1 + f_c = f_2 + C_2 + C_1 = \dots = f_N + C_N + C_{N-1} + C_{N-2} + \dots + C_2 + C_1 \quad (15)$$

Because $f = f_0$, equation (15) can be simplified as shown in equation (16):

$$f = f_N + \sum_{i=1}^N C_i \quad (16)$$

The above equations illustrate the concept of the Mallat pyramid algorithm—namely, the concept of multiresolution analysis (Hu, et al., 1999, p. 19). Therefore, any function $f \in L^2(W)$ can be completely reconstructed using the low-frequency component; i.e., the “coarse image” part of f at resolution 2^{-k} and the high-frequency component; i.e., the “detail” part of f at resolution 2^{-k} ($1 \leq k \leq N$).

WAVELET DENOISING PRINCIPLES

In this section, we discuss three wavelet denoising methods:

Wavelet threshold denoising: Wavelet threshold denoising is the default threshold for the signal generated using the `ddencmp` function, followed by denoising performed using the `wdencomp` function (Xu et al., 2021).

Hard denoising: When this method is used, all the high-frequency coefficients in the wavelet decomposition structure are set to zero, effectively removing the high-frequency components. Subsequently, the signal is reconstructed (Ou & Yang, 2023). This method is convenient, resulting in a smooth denoised signal, but it may cause a loss of useful signal components.

Given soft (hard) threshold denoising: When this method is used, threshold values can be obtained using empirical formulas; these formulas are more reliable than default thresholds (He, 2023).

Wavelet Denoising Process

An important application of wavelet analysis is the exploitation of the multiresolution analysis properties of wavelets to denoise images and signals. Typically, a noisy two-dimensional image model is represented as shown in equation (17):

$$h(i, k) = u(i, k) + \sigma e(i, k) \quad i = 1, \dots, m; k = 1 \quad (17)$$

In equation (17), $h(i,k)$ represents the observed value (i.e., an image containing noisy content), $u(i,k)$ represents the desired image signal (i.e., the real image), $e(i,k)$ stands for higher-order white noise $N(0,1)$ with a noise level of 1, and σ denotes the variance (Xu, 2023).

In engineering applications, low-frequency or steady signals typically represent useful signals, whereas high-frequency signals usually represent noise signals. Based on the characteristics of these common signals, the denoising process can be described as follows:

First, the wavelet signal is decomposed as shown in Figure 1, where C_1 , C_2 , and C_3 contain the noisy components. After appropriate thresholds to the wavelet coefficients are applied, the denoised signal is then reconstructed, and finally, the real signal $u(i,k)$ is extracted from $h(i,k)$ (Wang et al., 2023).

Two-Dimensional Image Denoising

In general, the above denoising steps can be divided into the following stages:

First, for the aforementioned wavelet decomposition of the image signal, a wavelet is selected and its decomposition order is set to N . Subsequently, the signal h undergoes N levels of wavelet decomposition (Yang et al., 2023).

Second, threshold quantization of wavelet decomposition high-frequency coefficients is performed; that is, threshold quantization is carried out by choosing a threshold for each layer from the first layer to the n th layer (Tang et al., 2023).

Third, two-dimensional wavelet reconstruction is carried out; that is, low-frequency coefficients are obtained from the n th layer of wavelet decomposition, followed by obtaining high-frequency coefficients from the first layer to the n th layer. Next, two-dimensional image wavelet reconstruction is performed on the coefficients (Zheng, 2022).

Of these three stages, the most crucial part is to choose the threshold and quantize it. Note that these factors will directly determine the signal denoising quality (Hai et al., 2023).

Design of the Wavelet Local Threshold Denoising Algorithm

The wavelet local threshold denoising algorithm design is based on a technique of selecting two-dimensional wavelet thresholds from images. It determines the local thresholds by using the characteristics of different directional high-frequency wavelet coefficients (Wang et al., 2023).

Noise Characteristics Under Wavelet Transform

In this section, we describe four theorems related to noise characteristics under wavelet transform.

Theorem 1

Low-frequency signals or relatively smooth signals are often useful signals, whereas high-frequency signals are often noise signals. Band limitation is one of the characteristics of useful signals, where they are concentrated over a small portion of the phase space. In other words, only a small portion of wavelet coefficients contribute to the signal's energy.

Theorem 2

In wavelet decomposition coefficients, both high/low wavelet coefficients and low/high wavelet coefficients contain low-frequency components. The magnitudes of most of these coefficients are greater than the magnitudes of high/high wavelet coefficients (Ou & Yang, 2023).

Theorem 3

Let $n(i)$ be a zero-mean white noise sequence so that under the wavelet transform, it remains a zero-mean sequence. White noise sequences with equal variances are also coefficient sequences under the wavelet basis. Specifically, when $n(i)$ is a Gaussian white noise sequence, its wavelet basis coefficients are also Gaussian white noise sequences with variance identical to that of the original sequence.

Theorem 4

The wavelet decomposition coefficients of Gaussian white noise are independent and Gaussian distributed (Chen, 2023).

In other words, wavelet coefficients are uniformly distributed across different parts of the phase plane, and various wavelet coefficients contain the noise contribution.

Design of Two-Dimensional Wavelet Threshold Noise Filter

Let $\delta(t) \in L^2(W)$, where $L^2(W)$ is a square-integrable real space as well as a signal space with finite energy.

Let the Fourier transform of $\delta(t)$ be $\delta(\omega)$ if $\delta(\omega)$ satisfies the conditions shown in equation (18):

$$Q_\delta = \int_w \frac{|\hat{\delta}(\omega)|^2}{\omega} d\omega < \infty \tag{18}$$

Consider $\delta(t)$ as the fundamental or mother wavelet. A wavelet sequence can be obtained by translating and scaling the mother function $\delta(t)$.

In the discrete case, the wavelet sequence includes the formula shown in equation (19):

$$\delta_{k,l}(t) = 2^{-K/2} \delta(2^{-k}t - l) \quad k, l \in X \tag{19}$$

In the following case, the continuous wavelet transform of function $f(t) \in L^2(W)$ is given as shown in equation (20):

$$P_f(a,b) = \langle f, \delta_{a,b} \rangle = |a|^{-1/2} \int_w f(t) \delta\left(\frac{t-b}{a}\right) dt \tag{20}$$

The above inverse transformation is as shown in equation (21):

$$f(t) = \frac{1}{Q_\delta} \int_w \int_w \frac{1}{a^2} P_f(a,b) \delta\left(\frac{t-b}{a}\right) da db \tag{21}$$

From the above equations, note that the algorithm for one-dimensional signal decomposition is similar to that for two-dimensional image wavelet decomposition. Both the scaling function and the two-dimensional wavelet function are obtained through the one-dimensional wavelet function and tensor product transformation (Liu, 2023).

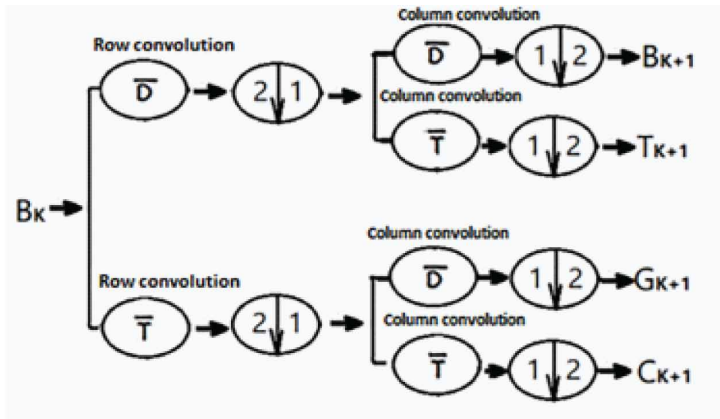
Two-Dimensional Wavelet Decomposition

Two-dimensional wavelet decomposition decomposes the low-frequency part of scale function k into four parts: the low-frequency part of scale $k+1$, and the high-frequency parts in three directions: vertical, horizontal, and oblique.

Figure 2 shows the basic decomposition steps.

Here is a summary of the symbols in Figure 2:

Figure 2. Schematic Diagram of Fast Wavelet Algorithm



Note. Source: Hu, et al. (1999), p. 69.

- $2 \downarrow 1$ equals column sampling, retaining even-numbered columns.
- $1 \downarrow 2$ equals row sampling, retaining even-numbered rows.
- \bar{D} equals row convolution, performing convolution operations with. It is low-pass filter.
- \bar{D} or \bar{T} equals filters.
- \bar{T} equals column convolution, performing convolution. It is high-pass filter.
- operations with \bar{T} or \bar{D} filters.

According to the process illustrated in Figure 2, the input image B_k undergoes the wavelet transform, resulting in four sub-images named as the horizontal sub-image T_{k+1} , the smooth sub-image B_{k+1} , the diagonal sub-image C_{k+1} , and the vertical sub-image G_{k+1} .

Subsequently, the horizontal sub-image T_{k+1} undergoes two filtering processes that allow low-frequency components in the horizontal direction and high-frequency components in the vertical direction to pass through.

Note that based on the above procedure, the vertical sub-image G_{k+1} contains the high-frequency and low-frequency components in the horizontal and vertical directions, respectively. The diagonal sub-image C_{k+1} contains high-frequency components in both the horizontal and vertical directions.

Hence, the horizontal sub-image T_{k+1} , the vertical sub-image G_{k+1} , and the diagonal sub-image C_{k+1} usually contain the noise component. Subsequently, threshold processing is applied to the aforementioned wavelet coefficients. Wavelet coefficients greater than this threshold are considered as transformations containing both signal and noise, and they can be retained (simply retained or subjected to further operations). However, coefficients smaller than this threshold can be regarded as entirely derived from noise transformation. Removing these coefficients and then reconstructing the signal can achieve denoising results.

Because most of the wavelet signals containing the signal are preserved, the parts of the image that contain details are also well retained. Meanwhile, as low-frequency coefficients are obtained by wavelet decomposition and contain some noise, threshold processing is also necessary for these coefficients (Xu, 2023).

Above is a “ $m \times n$ ” two-dimensional model containing Gaussian white noise, which can be represented as shown in equation (22):

$$h(i, k) = u(i, k) + \sigma n(i, k) \quad i = 1, \dots, m; k = 1, \dots, n \quad (22)$$

Let P denote the transformation matrix of the discrete wavelet transform. Applying the formula in equation (22) for wavelet transformation then yields the values shown in equation (23):

$$H(i, k) = U(i, k) + N(i, k) \quad (23)$$

Equation (23) can be expanded as shown in equation (24):

$$H(i, k) = P(i, k), U(i, k) = Pu(i, k), N(i, k) = P\sigma n(i, k) \quad (24)$$

A transformation inverse matrix S exists that corresponds to P and satisfies PS = 1. For the order $\hat{u}(i, k)$ ($i = 1, \dots, m; k = 1, \dots, n$).

The prediction of $u(i, k)$ ($i = 1, \dots, m; k = 1, \dots, n$) based on the criterion of minimizing the mean squared error is denoted by $\hat{u}(i, k)$ ($i = 1, \dots, m; k = 1, \dots, n$), which is obtained by minimizing the risk function $W(u, \hat{u})$ as shown in equation (25):

$$W(\hat{u} - u) = \frac{1}{m * n} E \left\| \hat{u} - u \right\|^2 = \frac{1}{m * n} \sum_{i=1}^m \sum_{k=1}^n E \left(\hat{u} - u \right)^2 \quad (25)$$

Let $I_n = \{1, \dots, m\}$, $H \subset I_n$, $K_n = \{1, \dots, n\}$, $V \subset K_n$.

The definition is calculated as shown in equation (26):

$$\begin{cases} \omega_{ik} & i \in H, k \in V \\ \left(\hat{u}^{HV}(\omega) \right)_{ik} & = \\ 0 & i \notin H, k \notin V \end{cases} \quad (26)$$

In equation (26), $(\hat{u}^{HV}(\omega))_{ik}$ is a selection estimator and has the elements shown in equation (27):

$$W(\hat{u} - u) = E \left\| \hat{u}^{H,V} - u \right\|^2 = \min_{H,V} \left(\sum_{i \notin H} \sum_{k \notin V} U_{i,k}^2 + \sum_{i \in H} \sum_{k \in V} \sigma^2 \right) = \sum_i \sum_k \min \left(U_{i,k}^2, \sigma^2 \right) \quad (27)$$

In equations (26) and (27), $(\hat{u}^{HV}(\omega))_{ik}$ is a selection estimator.

Estimator selection is used to maintain the value of $|\ln(i, k)|$ greater than the weight ω_{ik} corresponding to variance σ , where ω_{ik} is estimated from $u(i, k)$. Assume that the noise predominates, then when $u(i, k)$ is less than the noise variance σ , it is “removed” and estimated as zero. Attaining a perfect estimator is not possible; however, extreme values of the error range can be provided (Xiao, 2023).

Adaptive threshold selection is a crucial step in wavelet threshold denoising methods. Because noisy images are decomposed using wavelets, applying the wavelet transform to high-frequency coefficients reveals both noise and image details, which have relatively small magnitudes. If a single threshold is chosen that is too small, most high-frequency coefficients become zero, resulting in the loss of image details. Hence, designing a denoising method that preserves image details while reducing image noise is necessary. The key to an effective design lies in the threshold selection.

Thus, in the context described above, we propose a method called the wavelet local thresholding, as shown in equation (28).

High/high wavelet value:

$$t = \sigma\sqrt{2\log N} \quad (28)$$

In equation (28), N is the number of pixels in the image, and σ is the variance of noise.

The coefficients of low/high wavelets and high/low wavelets have amplitudes greater than those of high/high wavelets; thus, the threshold shown in equation (29) is chosen:

$$t = l\sigma\sqrt{2\log N} \quad (29)$$

In equation (29), l is a constant ($l > 1$) whose value is adaptively chosen based on image quality metrics, such as peak signal-to-noise ratio (PSNR) and signal-to-noise ratio (SNR) (Huang et al., 2023).

Because the noise level is unknown, the scale is estimated as shown in equation (30):

$$\hat{\sigma} = \frac{S}{0.6674} \quad (30)$$

In equation (30), the absolute value of the median of appropriately normalized fine-scale wavelet coefficients is denoted as S . To summarize the above content, the self-determined method can be calculated as follows:

First, estimate $u(i, k)$ —that is, the denoised signal $\hat{u}(i, k)$ —which is obtained via the inverse wavelet transform of the thresholded coefficients $\hat{u}(i, k)$ (Jiang et al., 2023); that is, as shown in equation (31):

$$\hat{u}(i, k) = S\hat{u}(i, k) \quad (31)$$

Second, for wavelet coefficients $Y(i, k)$, choose a threshold t in the wavelet domain so that the coefficients greater than t are set to zero; otherwise, they remain unchanged. Obtain $\hat{u}(i, k)$.

Third, obtain the wavelet transform of the observation $h(i, k)$, where the wavelet coefficients are given as $Y(i, k) = P h(i, k)$.

APPLICATION OF MACHINE DIAL RECOGNITION

Denoising of Simulated Noisy Images

For this process, we simulated the car dashboard image using MATLAB 6.1. The steps are as follows:

First, we denoised images containing Gaussian white noise with variance between 0 and 1 using hard thresholding, soft thresholding, median filtering, `wdencomp` function, and wavelet local thresholding method (with $l = 3$) in this experiment.

Second, we chose two metrics, PSNR and SNR, to test the denoising effectiveness and validate the results of the simulation experiment, as shown in equations (32) and (33):

$$SNR = -10 \log_{10} \frac{\sigma^2}{c} \tag{32}$$

$$PSNR = -10 \log_{10} \frac{255^2}{c} \tag{33}$$

These equations can be used in the calculation shown in equation (34):

$$C = \frac{1}{S * N} \sum_{i=0}^{S-1} \sum_{k=0}^{N-1} (u_{i,k} - \hat{u}_{i,k})^2 \tag{34}$$

In equation (34), $u_{i,k}$ and $\hat{u}_{i,k}$ represent the pixel values of the original and reconstructed images, respectively.

Tables 1 and 2 compare actual and denoised experimental data obtained using hard thresholding, soft thresholding, median filtering, wdencomp function, and wavelet local thresholding methods ($\sigma = 0.01$, $\sigma = 0.02$). Figure 3 shows noise removal results for a car instrument panel image.

Here is a summary of the sections of Figure 3:

- (a) Captured image awaiting experiment
- (b) Original image
- (c) Noisy image
- (d) Image after noise removal using hard thresholding
- (e) Image after noise removal using soft thresholding
- (f) Image after noise removal using wdencomp
- (g) Image after noise removal using median filtering
- (h) The image after wavelet denoising with local thresholding

Note that Figure 3(a) is composed of two separate instrument images cropped from the original car instrument image, and Figure 3(b) is the original image for the experiment starting from Figure 3(a). Figure 3(c) shows the image with noise added to the image shown in Figure 3(b), and Figure 3(d) is the denoised image obtained using hard thresholding on Figure 3(c). Figure 3(e) is the image denoised using soft thresholding on Figure 3(c), and Figures 3(f) and 3(g) are the images denoised

Table 1. Experimental Data ($\sigma = 0.01$, $\sigma = 0.02$): Before Noise Reduction, Hard Threshold Noise Reduction, and Soft Threshold Noise Reduction

Variance Noise elimination method	$\sigma = 0.02$		$\sigma = 0.01$	
	PSNR	SNR	PSNR	SNR
Hard threshold noise elimination	16.2046	3.8267	20.077	6.6161
Soft threshold noise elimination	16.2903	3.8352	20.081	6.6213
Before noise reduction	16.2811	3.6384	20.078	6.6162

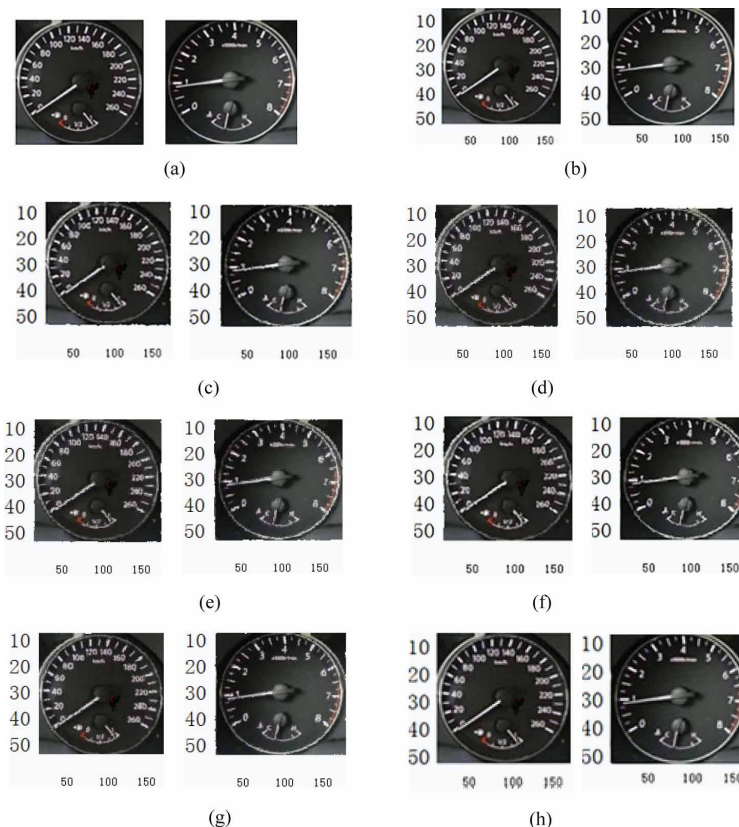
Table 2. Experimental Data ($\sigma=0.01, \sigma=0.02$): Wdencmp-Based Noise Elimination, Median Noise Cancellation, and Wavelet Local Threshold Denoising Method

Variance Noise elimination method	$\sigma = 0.02$		$\sigma = 0.01$	
	PSNR	SNR	PSNR	SNR
Wdencmp noise elimination	18.1224	5.6572	20.022	6.969
Median noise cancellation	20.2423	7.8032	22.931	9.4771
Wavelet local threshold denoising method	20.8083	8.2524	23.721	10.267

using wdencmp and median filtering on Figure 3(c), respectively. Figure 3(h) is the denoised image obtained using the method proposed in this paper on Figure 3(c). It is intuitively evident from these figures that the denoising performance of the proposed method is optimal.

Specifically, the results in Figure 3(d) show denoising using the hard thresholding method, which results in the loss of fine details and image blurring. Figure 3(e) shows the denoising results obtained after soft thresholding; these results exhibit loss of some fine features, especially causing blurriness in the numerical images on the dial. Figure 3(f) shows the denoising results using wdencmp, which involves complex parameter selection and computational overhead that lead to longer denoising times and inadequate timeliness. Figure 3(g) represents the images obtained after median filtering

Figure 3. Noise Removal Results on the Noisy Image ($\sigma=0.01$)



denoising; these images are smooth with blurry details. Figure 3(h) shows the denoising using the proposed wavelet local thresholding method, which demonstrates superior performance with good time efficiency. Therefore, the wavelet local thresholding denoising method proposed in this paper proves to be the most effective of the various methods used in the experiments.

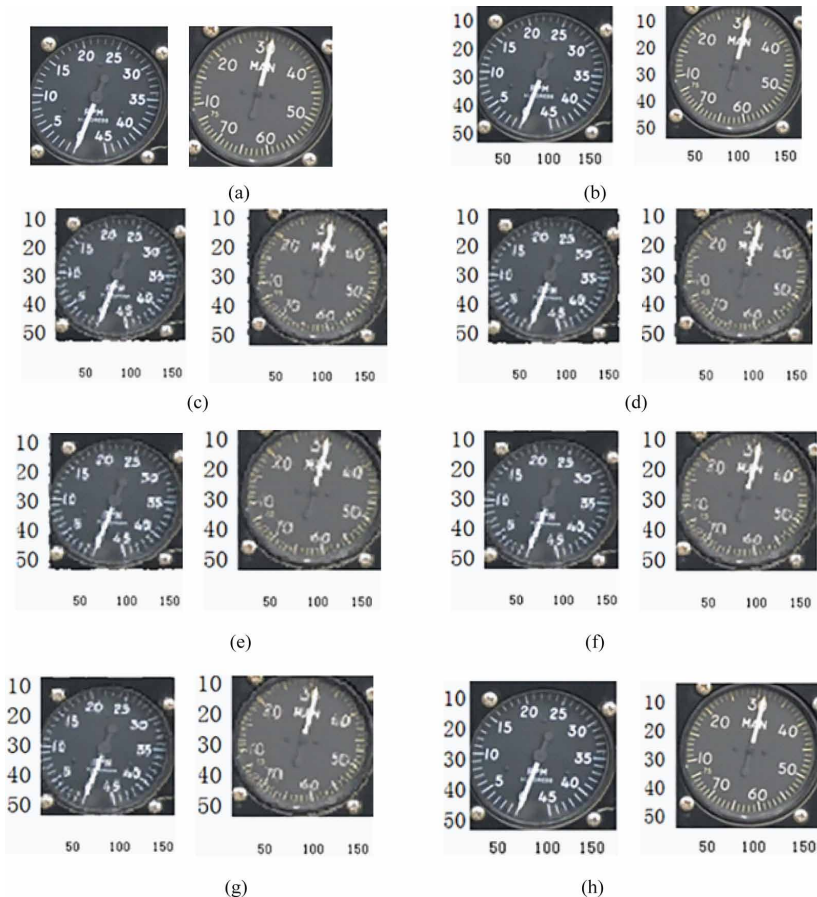
Figure 4 displays an aircraft instrument panel image.

Here is a summary of the sections of Figure 4:

- (a) Captured image awaiting experiment
- (b) Original image
- (c) Noisy image
- (d) Denoised image after hard thresholding noise reduction
- (e) Denoised image after soft thresholding noise reduction
- (f) Denoised image obtained after noise reduction using wdenomp
- (g) Denoised image after undergoing median noise reduction
- (h) The image after wavelet denoising with local thresholding

Figure 4(a) is composed of two separate instrument images clipped from the original aircraft instrument panel image. Figure 4(b) is the original image for the experiment obtained from Figure

Figure 4. Noise Reduction Results on the Noisy Image ($\sigma=0.01$)



4(a). Figure 4(c) is the noisy image obtained after adding the noise to the image in Figure 4(b). Figures 4(d) and 4(e) show the denoised images obtained using hard and soft thresholding on the image in Figure 4(c), respectively. Figure 4(f) shows the images denoised using wdencomp on Figure 4(c). Figure 4(g) is the image denoised using median filtering on the image in Figure 4(c), and Figure 4(h) is the image denoised using the method proposed in this paper. It is intuitively evident from Figure 4 that the method proposed in this paper has the optimal denoising performance.

Specifically, Figure 4(d) shows the denoising results obtained using the hard thresholding method, which exhibits the loss of fine details and image blurring. Figure 4(e) shows the denoised image obtained using the soft thresholding method, which suffers loss of some fine features, especially causing blurriness in the numerical images on the dial. Figure 4(f) shows the denoised results obtained using wdencomp that requires complex parameter selection, leading to computational overhead that causes longer denoising times and inadequate timeliness. Figure 4(g) represents the image after denoising with median filtering, which is smooth, but has blurry details. Figure 4(h) shows the denoising results obtained using the proposed method; these results demonstrate superior performance with good time efficiency. After comparing the performance of various methods used in the experiments, we note that the multiple wavelet coefficient method proposed in this paper proves to be the most effective.

Denoising of Real Noisy Images

Using MATLAB 6.1, we applied various custom methods, such as hard thresholding, soft thresholding, median filter, and wdencomp function, to images with unknown noise levels. A wavelet-based local thresholding method with $L = 3$ was implemented for denoising. Furthermore, in equation (18), the standard deviation $\hat{\sigma}$ of the high/high-frequency coefficients used by the aforementioned denoising methods $\hat{\sigma}$ could be considered an estimate of the noise variance σ .

The noise present in actual images is not necessarily additive, and therefore, in this case, the denoising effects of the aforementioned methods are not very pronounced, as seen in Figure 4. We further considered the case of binary images, where the binarization effect of the denoised image becomes crucial. Next, we show the binarization of the corresponding images obtained using the Otsu method, as well as the denoising performance of the aforementioned methods on these images. Figure 5(a) shows the panel image of a flying machine's dial.

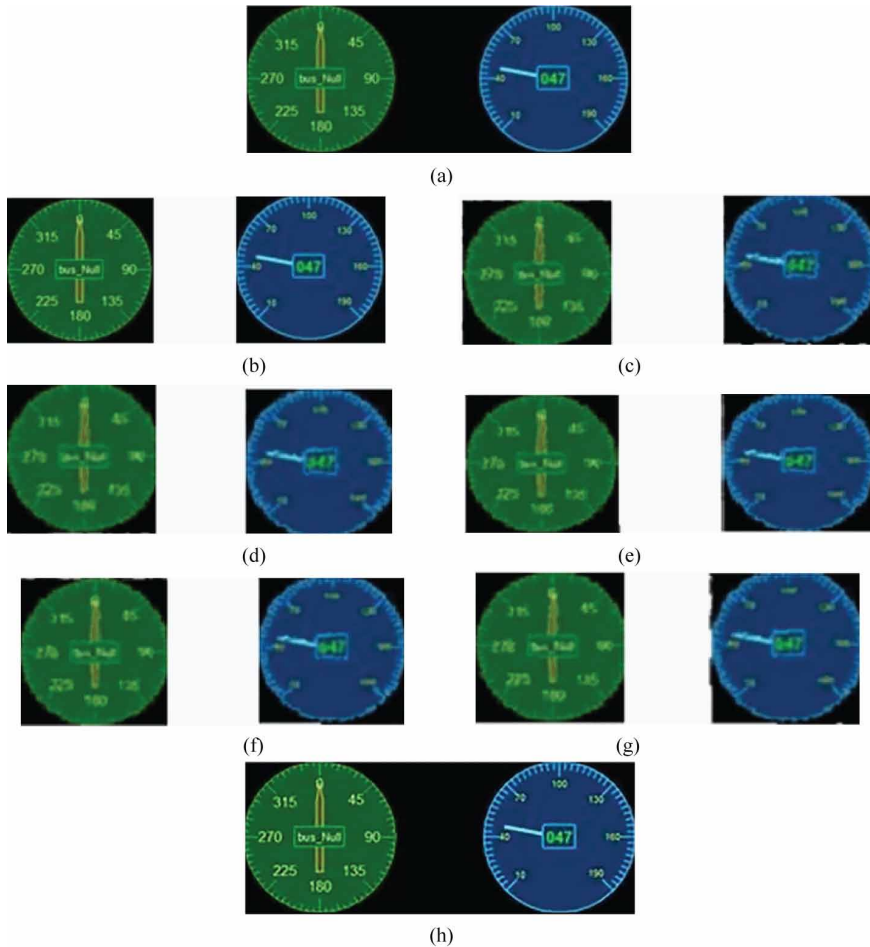
Here is a summary of the sections of Figure 5:

- (a) Actual panel image
- (b) Image to be processed
- (c) Original graphical binary image
- (d) Binary image after hard threshold denoising
- (e) Binary image after adaptive denoising
- (f) Binary image after soft threshold denoising
- (g) Binary image after median denoising
- (h) Binary image after denoising using the proposed method

Figure 5(b) is the image obtained by cropping the aircraft instrument panel image into two separate instrument images. Figure 5(c) shows the binarized version of the image in Figure 5(b). Figures 5(d) and 5(e) are the binary images after hard threshold and adaptive denoising of the image in Figure 5(c), respectively. Figures 5(f)–5(h) are the binary images obtained using soft threshold denoising, median denoising, and the proposed denoising method on the image shown in Figure 5(c), respectively.

Figure 5(d) shows the results of hard threshold denoising; these results can suffer from the loss of detailed information in the presence of high noise or rich image details. Figure 5(e) shows the results of adaptive denoising. These results have high computational complexity and may not be flexible enough for certain images. Figure 5(f) shows the results of soft threshold denoising, which

Figure 5. Denoising Performance on Binarized Images of a Flying Machine's Dial



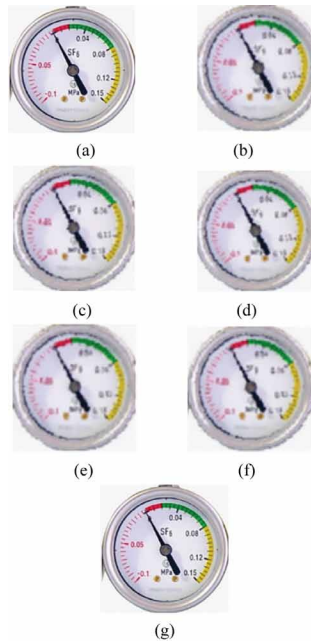
may fail to completely eliminate noise in the presence of high noise levels. Figure 5(g) shows the median denoising results. These results may have some impact on the overall brightness of the image in certain situations. Figure 5(h) shows the results of the denoising method proposed in this paper. This method exhibits better denoising performance and is more time-efficient than the other methods. Considering the various methods compared in Figure 5, we note that the wavelet-based local threshold denoising method proposed in this paper proves to be more effective.

Figure 6a shows an image of a robot's dial.

Here is a summary of the sections of Figure 6:

- (a) Image to be processed
- (b) Binarized actual image after adding noise
- (c) Binarized image after hard threshold denoising
- (d) Binarized image after adaptive denoising
- (e) Binarized image after soft threshold denoising
- (f) Binarized image after median denoising
- (g) Binarized image after denoising using the proposed method

Figure 6. Denoising Performance on Binarized Images of a Robot's Dial



For images affected by intense lighting, the performance degradation could have been caused owing to uneven illumination or overexposure, leading to abnormally high pixel values in certain areas. In the case of heavily contaminated images, the contaminants could obscure or distort image information, making it challenging for the denoising algorithm to accurately recover the original image. An in-depth analysis of these failure cases could help in identifying shortcomings of the proposed algorithm and guide future improvements. Potential enhancements to the algorithm might include incorporation of more complex denoising models to address the effects of lighting and contamination, as well as optimizing threshold selection strategies to adapt to different types of image noise and distortion (Zhou & Bu, 2023).

Table 3 compares the performance of the proposed method with that of other denoising techniques.

Note from Table 3 that the wavelet local threshold denoising method performs well in terms of denoising accuracy, but slightly lags deep learning denoising methods in handling complex noise. Furthermore, the method demonstrates high computational efficiency and interpretability. However,

Table 3. Comparison of Wavelet Local Thresholding, Median Filtering, Deep Learning Denoising Methods, and Wavelet Thresholding

Method	Denoising accuracy (%)	Computational efficiency	Interpretability	Ability to handle complex noise
Wavelet local threshold	98.04	Second highest	Strong	Moderate
Median filtering	97.50	Lowest	Weak	Strong
Deep learning denoising methods	96.80	Highest	Moderate	Strong
Wavelet thresholding	98.20	Second highest	Strong	Excellent

because of the lack of direct comparison data with other state-of-the-art methods, its performance evaluation in specific contexts requires further research and analysis (Zheng, 2022).

Denoising plays a crucial role in the field of image processing and computer vision. It enhances image quality and visual perception, making images clearer and more interpretable. It also improves the accuracy and robustness of subsequent image processing tasks, such as object detection and image segmentation. However, existing denoising techniques have certain shortcomings. Some methods may remove noise at the expense of image details, resulting in blurry or distorted images. Other methods may not perform well on certain types of noise, such as texture noise or speckle noise (Yang, et al. 2023). Additionally, some methods may require significant computational resources or complex parameter tuning, making them inefficient or difficult to implement. Therefore, evaluating the existing denoising techniques and their shortcomings for identifying the development direction of new methods and improving existing ones is crucial. An analysis of the pros and cons of existing techniques can better place the contributions of new methods within the broader research framework, providing guidance and insights for further advancements in the field of image processing (Xu, et al., 2021).

The wavelet local threshold denoising method has specific pros and cons compared with the latest deep learning methods.

The wavelet local threshold denoising method includes the following pros:

- **Simple implementation:** It is relatively simple, easy to implement and understand, requires a lower amount of annotated data, and has simple model structures.
- **High computational efficiency:** Compared with deep learning methods, the wavelet local threshold denoising method typically has a higher computational efficiency, especially when dealing with small-scale image data.
- **Strong interpretability:** The wavelet local threshold denoising method is more transparent. Its principles and denoising steps are easier to interpret, aiding in understanding the denoising process and results.

The wavelet local threshold denoising method includes these cons:

- **Limited denoising effect:** The wavelet local threshold denoising method may not be able to effectively handle complex noise and image structures. This limitation results in relatively poor denoising performance, especially in cases of high noise intensity or complex image details.
- **Weak generalization ability:** It typically requires manual selection of thresholds or parameters, resulting in a weak generalization ability and limited adaptability to different types and degrees of noise.
- **Inadequate handling of complex noise:** The wavelet local threshold denoising method may not effectively handle non-Gaussian noise or specific types of noise, such as texture noise or speckle noise.

In summary, although the wavelet local threshold denoising method has advantages such as simplicity, efficiency, and strong interpretability, it has limitations in handling complex image noise and structures (Sun, et al. 2020). In contrast, the latest deep learning methods can denoise complex image noise and structures more effectively with a higher generalization ability, but require more computational resources. Therefore, it is necessary to weigh the pros and cons of each image denoising method based on the specific situation and make a choice accordingly.

CONCLUSION

In this study, we focused on the image segmentation and recognition tasks for the dashboards of automobiles, airplanes, spacecrafts, and robotic instruments. We delved into the critical issues of

image preprocessing, specifically addressing noise reduction and distortion factors. We proposed and applied a method that used wavelet local thresholding for noise reduction to generate clear, undistorted images. This method provided a more reliable foundation for subsequent segmentation and recognition tasks. Initially, we recognized the crucial importance of denoising in image processing. The presence of noise could cause instability in segmentation and recognition algorithms, affecting the accuracy of the final results. By introducing the wavelet local thresholding method, we successfully reduced noise in the images, increasing the accuracy and reliability of subsequent processing.

The key innovation behind the proposed method was the fusion of features from different directional high-frequency wavelet coefficients with wavelet decomposition coefficients. The aim of this strategy was to precisely handle high-frequency information in different directions because different types of images might exhibit specific features in different directions. By integrating these features, we simultaneously improved the denoising performance and successfully preserved important image features, ensuring that high-quality images would be available as input to the final segmentation and recognition process.

Experimental results demonstrated the efficacy of our proposed wavelet local thresholding method in handling images of automobiles, airplanes, spacecrafts, and robotic instrument dashboards. One image out of a total of 102 images suffered significant distortion after denoising owing to intense lighting during capture. Because of strong light shining on the dashboard, another image was severely disturbed, resulting in incorrect image recognition. This is typically caused by light reflection and refraction, light spots and halos, reduced contrast, as well as light glare and shadows. However, the remaining instrument images resulted in highly satisfactory outcomes, with a denoising accuracy of 98.04%. Overall, compared to traditional denoising methods, our approach not only enhanced the image quality but also exhibited better performance in handling high-frequency information in different directions. This achievement could positively impact image segmentation and recognition accuracy.

ACKNOWLEDGMENT

This paper was collaboratively completed by Xiaoyuan Wang, Hongfei Wang, Jianping Wang, Maoyu Zhao, and Hui Chen. Among them, Xiaoyuan Wang, Hongfei Wang, and Jianping Wang conceived the ideas and conducted a substantial amount of experimental work. Under the guidance of Jianping Wang, Maoyu Zhao and Hui Chen conducted extensive research and organizational tasks. Xiaoyuan Wang prepared the initial draft, which was reviewed by Jianping Wang. Xiaoyuan Wang led the editorial work.

CONFLICTS OF INTEREST

We wish to confirm that there are no known conflicts of interest associated with this publication and there has been no significant financial support for this work that could have influenced its outcome.

FUNDING STATEMENT

No funding was received for this work.

REFERENCES

- Abudurehman, A. (2023). Design of a user comment management system based on text mining: Innovative organization management for e-commerce. [JOEUC]. *Journal of Organizational and End User Computing*, 35(1), 1–14. doi:10.4018/JOEUC.326611
- Chen, Q. (2023). Analysis of image processing technology based on computer vision algorithms. *Electronic Technology and Software Engineering*, (05), 178–181.
- Duan, Y. P., & An, Y. Y. (2021). Research on high-density mixed noise removal in images based on non local mean algorithm. [Theoretical Edition]. *Information and Computation*, 33(01), 25–26.
- Hai, Y. L., Egret, & Jiang, L. L. (2023). Design of image processing applications based on reconfigurable embedded computers. *Computer Programming Skills and Maintenance*, (03), 154–156.
- He, X. N. (2023). Application of image processing technology in web design. *Electron Technology*, 52(04), 280–281.
- Hu, C. H., Zhang, J. B., Xia, J., & Zhang, W. (1999). *System analysis and design based on MATLAB (wavelet analysis)*. Xidian University Press.
- Huang, J. M., Chen, P. P., & Wang, C. S. (2023). Research and implementation of OpenCV based image processing in Linux environment. *Computer Programming Skills and Maintenance*, (01), 143–146.
- Jiang, Y., Chen, X., Li, G., Wang, F., & Ge, H. (2023). Graph neural network and its research progress in field of image processing. *Computer Engineering and Applications*, 59(7), 15–30. doi:10.3778/j.issn.1002-8331.2205-0503
- Liu, L. L. (2023). Research on image processing technology based on embedded systems. *Information Recording Materials*, 24(03), 71–73.
- Lv, X., Chen, L. Q., Lu, Y. F., & Zhao, Y. F. (2021). A wavelet transform based anti cropping image encryption algorithm. [Natural Science Edition]. *Journal of Zhejiang Normal University*, 44(04), 56–62.
- Ou, B., & Yang, J. J. (2023a). Application of image processing technology in industrial automation systems. *Integrated Circuit Applications*, 40(03), 283–285.
- Ou, B., & Yang, J. J. (2023b). Prospects for image processing and recognition technology. *Electron Technology*, 52(04), 301–303.
- Sun, H., Zhao, W. Z., Zhao, W. H., & Duan, Z. Y. (2020). Research on edge distortion classification of tooth profile images based on improved twin support vector machines. *Guangzi Xuebao*, 49(10), 33–43.
- Sun, L. C., & Feng, H. Z. (2022). Image clarity processing based on encoding quantization parameter adjustment. *Jisuanji Fangzhen*, 39(04), 84–92.
- Sun, T. T., & Cui, S. H. (2020). Based on 3σ the application of wavelet thresholding method based on criteria in removing infrared image noise. [Natural Science Edition]. *Journal of Eastern Liaoning University*, 27(03), 201–204.
- Tang, Z. X., Li, W., & Yao, X. F. (2023). The application of traditional Chinese medicine image informatization project in medical image processing teaching. *Modern Distance Education of Traditional Chinese Medicine in China*, 21(07), 32–38.
- Wan, X. H., & Hao, R. J. (2022). Design and research of a mathematical model for noise removal in complex hyperspectral images. *Laser Journal*, 43(12), 113–116.
- Wang, J., Chen, K. J., Zhang, W. M., & Yu, N. H. (2023). Provable secure natural steganography for reversible image processing networks. *Chinese Journal of Image and Graphics*, 28(03), 107–119.
- Wang, X. Y., Zhu, K. Y., Zhang, W. W., & Wang, X. H. (2023). Design of underwater image processing software and quality evaluation system. *Electronic Design Engineering*, 31(07), 202–203.
- Xiao, Y. C. (2023). The application of mathematical morphology in digital image processing. *Integrated Circuit Applications*, 40(02), 297–299.

Xu, C. L. (2023). Design of wide-angle infrared image processing and communication circuit for power equipment in the cabinet based on FPGA. *Yangtze River Information and Communication*, 36(02), 144–146.

Xu, H. H., Zheng, J. W., Qin, M. J., & Chen, W. J. (2021). A noise removal algorithm for hyperspectral images optimized by structured matrices. *Journal of Computer-Aided Design and Graphics*, 33(01), 105–114.

Xu, L. L. (2023). The application of computer image processing technology. *Integrated Circuit Applications*, 40(04), 113–116.

Yan, J. B., Fang, Y. M., & Liu, X. L. (2022). A review of research on image quality evaluation — From the perspective of distortion. *Chinese Journal of Image and Graphics*, 27(05), 71–78.

Yan, J. H., Hou, P., Zhang, Y., Lv, X. Y., Ma, Y., & Wang, G. F. (2021). A method for judging single distortion type of image based on dual channel convolutional neural network. *Computer Applications (Nottingham)*, 41(06), 102–113.

Yan, L. (2023). A low-complexity channel estimation in Internet of Vehicles in intelligent transportation systems for 5G communication. [JOEUC]. *Journal of Organizational and End User Computing*, 35(1), 1–21. doi:10.4018/JOEUC.326759

Yan, Z. G., Tang, Y., Wang, X., & Chen, L. (2020). A distortion correction method for wellbore visualization detection images. [Natural Science Edition]. *Journal of Xi'an Shiyou University*, 35(06), 63–70.

Yang, S. P., Xu, C. C., Jie, Y. F., Zhou, G. Q., & Zhou, P. (2023). The non distortion condition of element images in optical field imaging. *LCD and Display*, 38(06), 42–49.

Yuan, G. M., Yang, G., Wang, J. F., Liu, H. J., & Wang, W. (2022). The application of multi-level wavelet transform in underwater image enhancement. *Optical Precision Engineering*, 30(22), 60–72. doi:10.37188/OPE.20223022.2939

Zhao, X. (2023). Deep mining technology of database information based on artificial intelligence technology. [IJITSA]. *International Journal of Information Technologies and Systems Approach*, 16(2), 1–13. doi:10.4018/IJITSA.316458

Zheng, R. D. (2022). Research on distortion analysis and quality evaluation of super-resolution images. *Broadcasting and Television Technology*, 49(09), 51–55.

Zhou, Y., & Bu, F. (2023). An overview of advancements in lie detection technology in speech. [IJITSA]. *International Journal of Information Technologies and Systems Approach*, 16(2), 1–24. doi:10.4018/IJITSA.325618

Xiaoyuan Wang (1966-), graduated from Hefei University of Technology in 2008 with a master's degree, is a senior experimentalist at Hefei College. Her research areas include electrical and electronic engineering, electrical automation, electromechanical integration, information and communication technology, etc. Two Chinese invention patents, and won the third prize in the first self-made experimental teaching instrument in Anhui Province in 2016.

Hongfei Wang (1994-), male, (Han ethnicity), Anhui native, Bachelor's degree, research area: software development. Obtained one Chinese invention patent and one utility model patent. Participated in writing 3 EI conference papers.

Jianping Wang (1955-), male (Han ethnicity), Professor, Anhui native, Ph.D., Ph.D. supervisor, Vice Dean of the School of Electrical and Automation Engineering at Hefei University of Technology, Director of the Institute of Intelligent Monitoring and Diagnosis, member of the school's Academic Committee, and director of the school's Academic Committee. Research areas: electrical and automation education and research.

Zhao Maoyu (1969-) male (Han ethnicity), native of Anhui Province, professor, Ph.D., master's supervisor, research areas: mold manufacturing technology, die-casting mold design, etc.

Chen Hui (1982-) female (Han ethnicity), native of Anhui Province, lecturer, master's degree, research area: college English teaching and research. Member of the Anhui Foreign Language and Literature Society.